# Coherent beam combination far-field measuring method based on amplitude modulation and deep learning

**Renqi Liu (刘人奇)[1,2], Chun Peng (彭 纯)[1], Xiaoyan Liang (梁晓燕)[1,3,*], and Ruxin Li (李儒新)[1,3,**]**

[1]*State Key Laboratory of High Field Laser Physics, Shanghai Institute of Optics and Fine Mechanics, Chinese Academy of Sciences, Shanghai 201800, China*

[2]*Center of Materials Science and Optoelectronics Engineering, University of Chinese Academy of Sciences, Beijing 100049, China*

[3]*School of Physical Science and Technology, ShanghaiTech University, Shanghai 200031, China*

**Corresponding author: liangxy@siom.ac.cn; **corresponding author: ruxinli@mail.shcnc.ac.cn*

Received October 28, 2019; accepted December 26, 2019; posted online April 10, 2020

A deep convolutional neural network is employed to simultaneously measure the beam-pointing and phase difference of sub-beams from a single far-field interference fringe for coherent beam combining systems. The amplitudes of sub-beams in the measurement path are modulated in order to prevent measuring mistakes caused by the symmetry of beam-pointing. This method is able to measure beam-pointing and phase difference with an RMS accuracy of about 0.2 μrad and $\lambda/250$, respectively, in a two-beam coherent beam combining system.

*Keywords: coherent beam combining; pattern recognition; deep learning.*

*doi: 10.3788/COL202018.041402.*

Ultra-intense and ultra-short lasers have made great progress on the basis of chirped pulse amplification (CPA) technology in recent years[1,2]. However, with the improvement of laser power, material damage has become the main factor limiting their development. As one of the most promising techniques to further improve laser output power, coherent beam combining (CBC) has attracted the attention of many laser researchers[3–7]. Several ultra-intense and ultra-short laser facilities have planned to employ the CBC technique, aiming to approach a 100 PW level output[2]. The most important problem in CBC is controlling the parameters that affect the combining efficiency. These parameters can be classified into two categories: dynamic parameters (including beam-pointing and phase difference) and static parameters (including group delay dispersion and wavefront aberrations, etc.). The former vary quickly with the environment conditions and need real-time adjustment, while the latter only depend on the system itself and need no dynamic feedback. Therefore, measuring beam-pointing and phase difference in real time is a key problem for effective CBC.

To date, several implementations of CBC based on the structure of ultra-intense and ultra-short lasers have been reported[7–9]. The common methods such as Hansch–Couillaud detectors[7], optical cross-correlators[8], and interference fringe patterns[9,10] are utilized to measure the phase difference in these systems. Nevertheless, the methods above can only measure the phase difference, and the beam-pointing is neglected. The research shows that the requirement of CBC on the beam-pointing stability is related to the beam diameter; the larger the beam diameter is, the higher the requirement for beam-pointing stability would be[11]. These experiments are all based on small beam diameters in which the beam-pointing has little effect on the combining efficiency. However, to achieve an ultra-intense and ultra-short output by CBC in the PW laser facility with a large beam diameter, beam-pointing is a crucial factor. Therefore, a method that can simultaneously measure the beam-pointing and phase difference is needed.

Here, we propose a method based on deep learning to concurrently measure the beam-pointing and phase difference in CBC systems since the interference fringe pattern of CBC contains the information of beam-pointing and phase difference of sub-beams. We employ a deep convolutional neural network (DCNN) trained by the amplitude modulated far-field fringe patterns in our method. Due to the considerable potential in image processing and computer vision tasks, such as image classification[12] and segmentation[13], the DCNN algorithm can distinguish the tiny change of far-field fringe pattern caused by the beam-pointing and phase difference. Moreover, the modulated amplitudes of sub-beams in the measurement path can prevent measuring mistakes caused by the symmetry of beam-pointing. Generally speaking, the two factors are measured separately in most CBC systems, while our method can measure the beam-pointing and phase difference of a multi-beam CBC system in one fringe pattern, which means that a lot of measurement elements can be saved. In this Letter, we mainly validate and analyze the method in a two-beam coherent combining system by simulation.

CBC can be categorized as two schemes, in general. One is a filled-aperture scheme commonly used in fiber lasers in which beams are overlapped on beam combiners, while the other is a tiled-aperture scheme in which beams are overlapped on the focal plane of the focusing elements. The difference between these two schemes is that the

 

sub-beams are spatially superposed on the near-field plane in the former but separated with a gap in the latter. Here, we only discuss the tiled-aperture scheme, which is appropriate for ultra-intense and ultra-short laser facilities. At the same time, we consider the use of a continuous reference light for measurements, as adopted in Ref. [9]. Taking Gaussian beams with a beam-pointing drift and phase difference in a near-field spatial coordinate, the $n$th beam distribution can be expressed as

$$E_n(x,y) = A_n(x,y)\exp[jk(x\cos\alpha_n + y\cos\beta_n) + j\varphi_n(x,y) + j\phi_n], \tag{1}$$

where

$$A_n(x,y) = A_n \exp\left[-\frac{(x-x_n)^2+(y-y_n)^2}{(D/2)^2}\right]. \tag{2}$$

$A_n$, $D$, $\varphi_n(x,y)$, and $(x_n, y_n)$ represent, respectively, the amplitude, beam diameter, wavefront phase, and position on the near-field plane of the $n$th beam. $\alpha_n, \beta_n, \phi_n$ are the beam-pointing on the $x$ axis and $y$ axis, and the phase of the $n$th beam, which vary quickly with the experiment conditions. According to the scalar diffraction theory, we can obtain the far-field intensity distribution after coherent combining on the focal plane of the lens as

$$I_\Sigma(u,v) \propto \left|\sum\nolimits_n \iint E_n(x,y)\exp[-jk(xu+yv)/f]\mathrm{d}x\mathrm{d}y\right|^2. \tag{3}$$

In the tiled-aperture scheme, the CBC efficiency is commonly characterized by Strehl ratio, which is

$$\mathrm{SR} = \frac{{I_\Sigma}^{\mathrm{peak}}(u,v)}{\sum\limits_n {I_n}^{\mathrm{peak}}(u,v)}, \tag{4}$$

where ${I_\Sigma}^{\mathrm{peak}}(u,v)$ represents the peak intensity of the coherent combined fringes, and ${I_n}^{\mathrm{peak}}(u,v)$ represents the peak intensity on the focal plane of the $n$th sub-beam.

Previous studies[11] have shown that in order to achieve a 95% CBC efficiency, the phase difference between the sub-beams should not exceed 0.22 rad, and the beam-pointing of each beam should not exceed 4.8 μrad (spot diameter is 10 mm), when the influence of various factors is considered separately for the CBC of $N(N \gg 1)$ beams. It should be noted that, with the increase of the spot diameter, the allowable error of beam-pointing for the same CBC efficiency would be smaller, which is basically inversely proportional.

As a structure of deep learning, the deep convolutional neural network is greatly effective in image processing. It uses a local receptive field, weighs sharing and pooling technology, and greatly reduces the training parameters compared to the neural network. In order to exploit a high-precision and reliable measurement method based on DCNN, an excellent model should first be trained. Increasing the depth or width of the model is the safest way to get a good model, but it leads to the increasing training cost. Thus, choosing an existing well-trained model is a better choice.

In our approach, we employ Inception-v3 as a training model to save training time and cost, which is an efficient computing DCNN model developed by Google[14]. According to the method of transfer learning, we keep the parameters of the previous layers, remove the last layer of the Inception-v3 model, and then retrain the last layer. The input of DCNN is the simulated far-field interference patterns, and the output is the beam-pointing and phase difference of each corresponding sub-beam.

A simple schematic diagram of a two-beam tiled-aperture CBC system is shown in Fig. 1(a). In this scheme, the beam-pointing and phase difference are commonly measured in front of the focusing element by the measurement system. We simulate the far-field interference patterns in the measurement system that change with different beam-pointing and phase according to Eq. (1). In this process, a Gaussian transverse intensity distribution and a constant wavefront $[\varphi_n(x,y)=0]$ of each sub-beam are assumed. This assumption can significantly simplify the computation, and the impact of the wavefront will be analyzed later. For convenience, the phase value of the first sub-beam $\phi_1$ is set as 0 as a reference, and the phases of other channels are randomly taken in the range of $[-\pi, \pi]$. The values of beam-pointing of all sub-beams $[\alpha_n, \beta_n]$ are randomly taken in the range of $[-20\ \mu\mathrm{rad}, 20\ \mu\mathrm{rad}]$. Particularly, in order to prevent measurement mistakes caused by the symmetry of beam-pointing, we modulate the amplitude of each sub-beam, which means taking different values for $A_n(x,y)$. It is easy to accomplish in experiment with an amplitude modulation element in the measurement path, leaving no impact on the main optical path, as shown in Fig. 1(a).

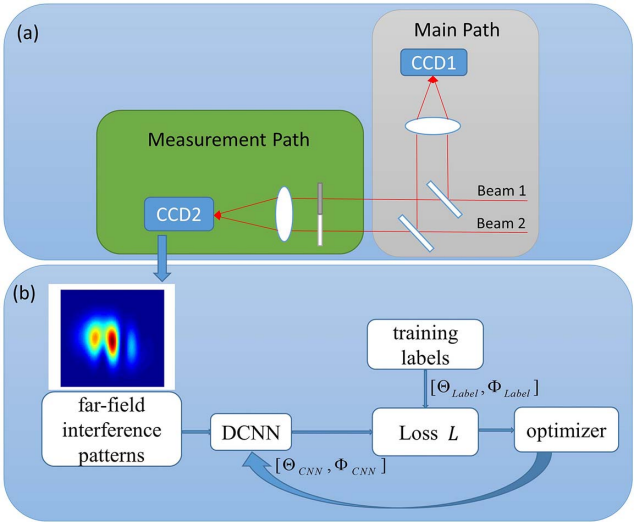


Fig. 1. (a) A simple schematic diagram of a two-beam tiled-aperture CBC system and (b) the training procedure of DCNN.

Further, a sampling window with a proper size is needed to ensure the measurement range of beam-pointing and, at the same time, a less amount of computation. In our case, we choose the size of $100 \times 100$ to sample the far-field interference patterns. In addition, the sampling images should be extended to the size of $100 \times 100 \times 3$, due to the fact that the input layer of the Inception-v3 model can only receive color images in RGB format. Finally, considering the accuracy of the model and the computation amount, 20,000 far-field interference patterns and corresponding labels are generated, of which 70% are used as the training set, 30% as the validation set, and 500 additional samples are generated as the testing set.

The training process of the deep convolutional neural network is shown in Fig. 1(b). It can be divided into two stages, the forward propagation stage and the back propagation stage. In the forward propagation stage, the input layer receives the far-field interference patterns and the output layer exports a list of prediction arrays that will be compared with the corresponding labels to calculate the loss of DCNN according to the loss function $L$. In this process, multiple convolution layers and pooling layers extract the input image features with multiple dimensions and compress them, while the activation layer can introduce nonlinearity. In the back propagation stage, the gradient of the neurons in all the hidden layers is calculated by the loss, and a gradient descent algorithm is used to update the weights of all the neurons. Through the iteration of the two processes, the DCNN loss is minimized to a desired value.

Loss function is the key factor for the training of DCNN, and thus, choosing an appropriate loss function is significant for high measurement accuracy. In our case, the measurement accuracy of beam-pointing and phase difference is of a different order of magnitude, and the loss function can be defined as

$$L = \|\Theta_{\text{CNN}} - \Theta_{\text{label}}\|^2 + \gamma^2 \|\Phi_{\text{CNN}} - \Phi_{\text{label}}\|^2, \quad (5)$$

where $\Theta = [\alpha_1, \beta_1, ..., \alpha_n, \beta_n]$, $\Phi = [\phi_2, ..., \phi_n]$, the unit of $\Theta$ is μrad and of $\Phi$ is rad. The list $[\alpha_1 \beta_1, ..., \alpha_n \beta_n, \phi_2, ..., \phi_n]$ represents the beam-pointing and phase difference of each example. The subscripts CNN and label represent the values calculated by the deep convolutional neural network and the values of the input labels, respectively. The parameter $\gamma$ is a normalization factor between beam-pointing and phase difference, which has an important impact on the training result.

In this Letter, the coherent beam combination of two quasi-monochromatic beams (800 nm) is considered. When simulating the far-field interference fringe, every parameter in Eq. (4) can affect the shape of the far-field pattern, besides the beam-pointing and phase difference. Here, we choose one condition as an example. On the near-field plane, the diameter of each beam is 10 mm, and the gap between the two beams is 10 mm. The focal length is 1000 mm, and the resolution of the far-field record is 2 μm. An area with $100 \times 100$ pixels is chosen as the sampling window of the interference fringe.

According to the parameters above, we simulate several far-field interference fringes under different beam-pointing and phase difference values $[\alpha_1, \beta_1, \alpha_2, \beta_2, \phi_2]$, as shown in Fig. 2. It indicates that the beam-pointing and phase difference make different contributions to the shape of the far-field interference fringe. Beam-pointing separates the fringe and shifts the spot center, while the phase difference moves the fringe series. Thus, the DCNN can identify these two factors, respectively, taking them as two features of the far-field images. However, due to the symmetry of beam-pointing, we cannot distinguish which beam has a beam-pointing drift when the two beams are basically the same ($A_2 = A_1$), as shown in Figs. 3(a) and 3(b). The two far-field patterns are the same when the same beam-pointing drift occurs in either beam. Such a problem can be solved by modulating the amplitudes of different beams, for instance, the result is different when $A_2 = 2A_1$, as shown in Figs. 3(c) and 3(d). Therefore, the amplitude modulation is a pre-requisite point in our method to code the sub-beams in the measurement system.

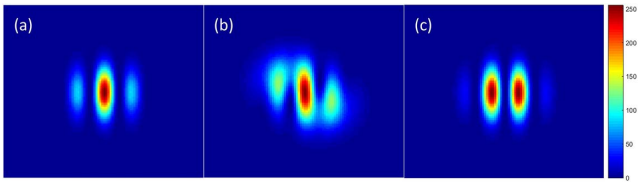


Fig. 2. Far-field distribution under different beam-pointing and phase differences: (a) $[0, 0, 0, 0, 0]$, (b) $[20\ \mu\text{rad}, 20\ \mu\text{rad}, -20\ \mu\text{rad}, -20\ \mu\text{rad}, 0]$, and (c) $[0, 0, 0, 0, \pi]$.

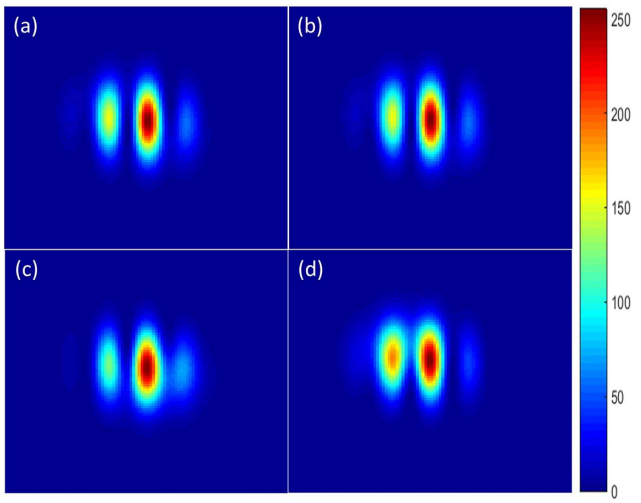


Fig. 3. Far-field distribution under different amplitude modulation ratios: (a) $A_2 = A_1$, $[20\ \mu\text{rad}, 20\ \mu\text{rad}, 0, 0, 0]$, (b) $A_2 = A_1$, $[0, 0, 20\ \mu\text{rad}, 20\ \mu\text{rad}, 0]$, (c) $A_2 = 2A_1$, $[20\ \mu\text{rad}, 20\ \mu\text{rad}, 0, 0, 0]$, and (d) $A_2 = 2A_1$, $[0, 0, 20\ \mu\text{rad}, 20\ \mu\text{rad}, 0]$.

In the training process, the RMSPropOptimizer algorithm is employed, and the value of $\gamma$ in the loss function is 10. In this case, 20,000 simulated far-field interference patterns are fed to our neural network model to obtain the training error curve, as shown in Fig. 4(a). It is found that the training error decreases with the increase of training epochs, while the validation error oscillates or even becomes larger. Thus, we use the early stopping method to save the computation time and to also prevent overfitting of DCNN. Here, we set the rule that when the value of the loss function $L$ falls to less than 0.1 in 30 epochs, the training process stops, and the best network parameters are achieved. Finally, the testing set is put into the trained DCNN, the beam-pointing and phase difference are measured by this optimized network, and the absolute value of the measurement errors can be illustrated by a scatter diagram, as shown in Fig. 4(b).

The RMS errors between the predictions of the network and label values of the 500 testing samples are $[0.192\ \mu\text{rad}, 0.181\ \mu\text{rad}, 0.182\ \mu\text{rad}, 0.193\ \mu\text{rad}, 0.0243\ \text{rad}]$. We choose the maximum value from the four beam-pointing errors (0.192, 0.181, 0.182, 0.193) to evaluate our beam-pointing measurement accuracy in this Letter. Thus, in this case, our DCNN can measure beam-pointing with an accuracy of 0.193 μrad and phase difference with an accuracy of 0.0243 rad, which completely meet the measurement requirements in the CBC system.

There are several factors that have influences on the measurement accuracy in the DCNN method. It is mentioned that the value of $\gamma$ has an impact on the training result, because the loss function plays a decisive role in the training process. We choose four different values to compare the measuring errors, and the results are illustrated in Fig. 5 in which the percentage of each error level in testing set is shown by a bar diagram. We can find that the phase difference error decreases when the value of $\gamma$ increases in Fig. 5(b), while the beam-pointing error increases when the value is too high in Fig. 5(a). The results show that we can achieve a balance between these two errors when the value of $\gamma$ is around 10. $\gamma$ is the weight of the phase difference in the loss function and should be well chosen to balance the scale of the beam-pointing and phase difference. This skill, called normalization, is often used in the optimization process of neural networks to prevent the vanishing gradient problem and overfitting problem.

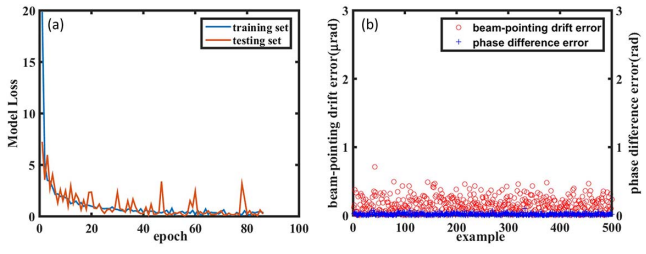


Fig. 4. (a) Training and validation errors across training epochs. (b) The testing set error of 500 samples; the red circle represents the beam-pointing error, and the blue sign represents the phase difference error.

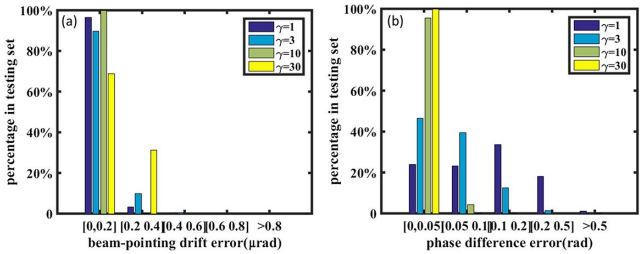


Fig. 5. Testing set error distribution, in the cases of $\gamma = 1$, $\gamma = 3$, $\gamma = 10$, and $\gamma = 30$: (a) the beam-pointing error and (b) the phase difference error.

Since amplitude modulation is a key step in our method, its effect on the training results should be analyzed. First, the modulation ratio $R = A_2/A_1$ is set as 1. The training procedure terminates in a short time with a divergence result, which proves the indiscernibility of the far-field fringe patterns in Figs. 3(a) and 3(b). Then, we also choose four different values of $R$, and the results are illustrated in Fig. 6. It shows that both beam-pointing and phase difference have the minimum error when the value of $R$ is around 2. We conclude that when the modulation ratio is close to 1, the difference in the fringe pattern is too small to distinguish, while when it is too large, the contrast of the fringe pattern decreases significantly, making the measurement accuracy decline. Thus, the value of $R$ should be moderate.

Through the simulation of the CBC theory, we know that the larger the beam diameter is, the smaller the beam-pointing drift is needed for identical combining efficiency. That is, the network is more sensitive to the beam-pointing when the beam diameter is larger. Here, we choose four beam diameter values and change the corresponding focal lengths to keep the value of the $F$ number ($F = f/D$) and the far-field spot size unchanged. Training the DCNN separately in these conditions, the testing results are illustrated in Fig. 7, where the corresponding beam-pointing errors and phase difference errors are $[0.294\ \mu\text{rad}, 0.0406\ \text{rad}]$, $[0.193\ \mu\text{rad}, 0.0243\ \text{rad}]$, $[0.132\ \mu\text{rad}, 0.0352\ \text{rad}]$, and $[0.129\ \mu\text{rad}, 0.0385\ \text{rad}]$, respectively. The results indicate that the beam-pointing

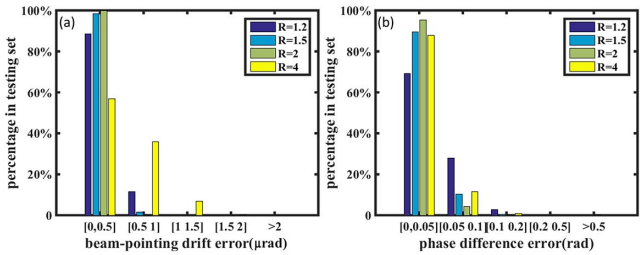


Fig. 6. Testing set error distribution, in the cases of $R = 1.2$, $R = 1.5$, $R = 2$, and $R = 4$: (a) the beam-pointing error and (b) the phase difference error.

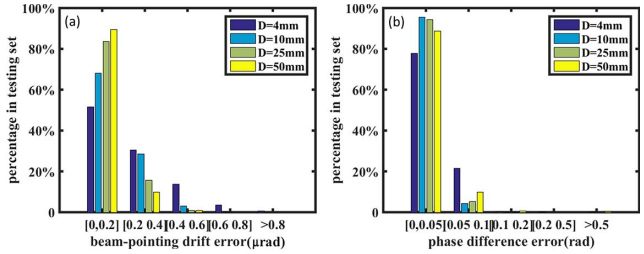


Fig. 7. Testing set error distribution, in the cases of $D = 4$ mm, $D = 10$ mm, $D = 25$ mm, and $D = 50$ mm: (a) the beam-pointing error and (b) the phase difference error.

**Table 1.** Measurement Errors Under Different Wavefront Aberrations

| Training Set Wavefront Aberration (rad) | Testing Set Wavefront Aberration (rad) | Beam-pointing Error (μrad) | Phase Difference Error (rad) |
|---|---|---|---|
| 0 | 0 | 0.193 | 0.0243 |
| | $\pi/4$ | 0.700 | 0.0308 |
| | $\pi/2$ | 1.530 | 0.0615 |
| $\pi/4$ | 0 | 0.346 | 0.0484 |
| | $\pi/4$ | 0.423 | 0.0444 |
| | $\pi/2$ | 0.983 | 0.0684 |

measurement accuracy will be higher with the increase of the beam diameter, while the improvement is limited when the diameter is large enough. This may be due to the limited pixel accuracy and bit accuracy.

When applying the method to the CBC experiment, the training set should be generated from the experimental data in which the wavefront aberration exists. Therefore, we should also discuss the impact of wavefront aberration on the measurement accuracy. Several testing sets with wavefront aberration of different peak-valley levels are generated and predicted by the previous trained DCNN. It is found that the beam-pointing error increases rapidly with the increasing testing set wavefront aberration, as shown in Table 1. The results indicate that the generalization performance will decay when the wavefront aberration is too large. We also retrain our network using a new training set with a larger wavefront aberration. The new network shows a better performance in which the difference between wavefront aberrations of the training set and testing set plays a major role. This problem can be solved by collecting training sets and testing sets in the same experiment conditions. In addition, to obtain a good performance of the measurement DCNN, we need to measure and reduce the wavefront aberration in the CBC experiment.

In conclusion, we present a far-field measuring method for CBC systems based on amplitude modulation and deep learning. This method can simultaneously measure the beam-pointing and phase difference of each sub-beam in a single far-field interference fringe pattern. A DCNN based on the amplitude modulated fringe patterns is trained, whose beam-pointing measurement RMS accuracy is about 0.2 μrad and the phase difference is about $\lambda/250$. The factors affecting the training result of the DCNN and the measurement accuracy, such as the normalization factor, amplitude modulation ratio, beam diameter, and wavefront aberration, are analyzed in detail. In addition, the method can also be applied to multi-beam coherent combining systems. This method has a potential application to measuring the beam-pointing and phase difference in ultra-intense and ultra-short CBC laser systems. We will employ the method in our next work to achieve the feedback from the beam-pointing and phase difference for CBC in experiment.

This work was supported by the National Natural Science Foundation of China (NSFC) (Nos. 61775223 and 11974367) and the Strategic Priority Research Program of Chinese Academy of Sciences (No. XDB1603).

## References

1. D. Strickland and G. Mourou, Opt. Commun. **56**, 219 (1985).
2. C. N. Danson, C. Haefner, J. Bromage, T. Butcher, J. C. F. Chanteloup, E. A. Chowdhury, A. Galvanauskas, L. A. Gizzi, J. Hein, D. I. Hillier, and N. W. Hopps, High Power Laser Sci. Eng. **7**, e54 (2019).
3. T. Y. Fan, IEEE J. Sel. Top. Quantum Electron. **11**, 567 (2005).
4. J. Bourderionnet, C. Bellanger, J. Primot, and A. Brignon, Opt. Express **19**, 17053 (2011).
5. A. Klenke, E. Seise, S. Demmler, J. Rothhardt, S. Breitkopf, J. Limpert, and A. Tünnermann, Opt. Express **19**, 24280 (2011).
6. S. J. Augst, T. Y. Fan, and A. Sanchez, Opt. Lett. **29**, 474 (2004).
7. S. N. Bagayev, V. E. Leshchenko, V. I. Trunov, E. V. Pestryakov, and S. A. Frolov, Opt. Lett. **39**, 1517 (2014).
8. J. Mu, Z. Li, F. Jing, Q. Zhu, K. Zhou, S. I. Wang, S. Zhou, N. Xie, J. Su, J. Zhang, X. Zeng, Y. Zuo, L. Cao, and X. Wang, Opt. Lett. **41**, 234 (2016).
9. C. Peng, X. Liang, R. Liu, W. Li, and R. Li, Opt. Lett. **44**, 4379 (2019).
10. R. Liu, C. Peng, W. Wu, X. Liang, and R. Li, Opt. Express **26**, 2045 (2018).
11. V. E. Leshchenko, Opt. Express **23**, 15944 (2015).
12. D. Ciresan, U. Meier, and J. Schmidhuber, in *IEEE Conference on Computer Vision and Pattern Recognition (CVPR)* (2012), p. 3642.
13. V. Badrinarayanan, A. Kendall, and R. Cipolla, IEEE Trans. Pattern Anal. Mach. Intell. **39**, 2481 (2017).
14. C. Szegedy, V. Vanhoucke, S. Ioffe, J. Shlens, and Z. Wojna, in *IEEE Conference on Computer Vision and Pattern Recognition (CVPR)* (2016), p. 2818.